EPSC2017

LF1 abstracts

EPSC Abstracts
Vol. 11, EPSC2017-13, 2017
European Planetary Science Congress 2017

In Situ Sampling of Terrestrial Dust Devils and Implications for Mars

J. Raack (1), D. Reiss (2), M.R. Balme (1), K. Taj-Eddine (3,4) and G.G. Ori (4,5)
(1) School of Physical Science, STEM, The Open University, Milton Keynes, UK, jan.raack@open.ac.uk, (2) Institut für Planetologie, Westfälische Wilhelms-Universität, Münster, Germany, (3) Géologie et Géoinformatique, Faculté des Sciences Semlalia, Université Cadi Ayyad, Marrakech, Morocco, (4) Ibn Battuta Centre, Faculté des Sciences Semlalia, Université Cadi Ayyad, Marrakech, Morocco, (5) International Research School of Planetary Sciences, Università "G. D'Annunzio", Pescara, Italy

1. Introduction and Background

Here we report on in situ sampling of the relative dust load and the vertical grain size distribution at different sample heights of several dust devils (DDs). The sampling occurred during two field campaign on rippled surfaces in the Sahara Desert in southern Morocco (2012: northwestern rim of the Erg Chegaga; 2016: plains east of Erg Chebbi). We present advantages and difficulties of such in situ sampling, the first published results from our 2012 field trip [1], and some implications for Mars.

DDs are small vertical convective vortices which occur on Earth and Mars [e.g.,2,3], and are formed by insolation under clear skies [3]. DDs consist of a low pressure region in the interior which is surrounded by tangential winds and updrafts [4,5]. These winds and updrafts lift particles (dust and sand) which makes them visible [3,6].

Particles entrained into the atmosphere by DDs have an influence on the climate and environment [3,7,8]. Lifted small aerosols (~<25 µm on Earth [3,7]; ~<20 µm on Mars [5]) can be entrained into the atmosphere in suspension and transported over long distances. Larger particles (sand-size) remain at lower heights and build-up the so-called “sand skirt” of the DDs [3,9], which reinforces their erosional ability. Their erosional potential can also be recognized by their ability to remove fine particles of the surface and rework the surface: observable as dark [e.g., 10,11] and bright [12] dust devil tracks on Earth and, more commonly, on Mars [e.g.,13,14].

2. Data and Methods

For our in situ sampling we used a 5 m high aluminium pipe with sampling areas made of removable adhesive tape on one side. This device was held upright, facing into the path of the DD [1]. After one passage of the dust devil, the sampling tape, which now had grains adhered to it, was preserved immediately on-site by sticking the sample patches onto glass slides. With this method we took samples of two DDs during the 2012 (sampling up to 2 and 4 m, sampling intervals 0.25 and 0.5 m), and six DDs during the 2016 field trip (sampling up to 5 m each, sampling intervals 0.5 m).

The maximum diameter of all particles at all sampling heights within a representative area of 0.5 cm^2 were measured using an optical microscope. Grain sizes were classified after [15].

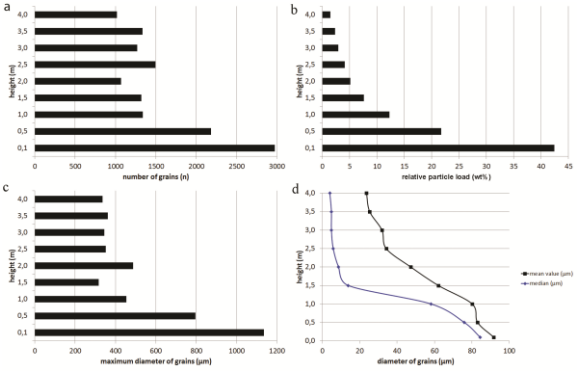

Figure 1: DD #1. **(a)** Number of measured grains, **(b)** relative particle load (wt%), **(c)** maximum diameter of grains, and **(d)** mean value and median of the diameter vs. height. From [1].

3. Results

An example of measuring results from DD #1 is presented in Fig. 1. The greatest number of particles (~36.8%) were sampled within the first 0.5 m (Fig. 1a). The relative particle load (wt%) shows a nearly exponential decrease of lifted particles with height (Fig. 1b). The largest grains sizes were found in the lowest 0.5 m, while above this the maximum grain sizes range between ~300 and ~500 µm (Fig. 1c). Median and mean values both decrease with height (Fig. 1d). Measurements for DD #2 show comparable results with only minor variations [1].

General grain size distributions for both DDs from clay to medium sand are comparable with some slight variations [1]. Both DDs show a relatively high amount of clay (~31.18% of lifted particles for DD #1, ~35.8% for DD #2), a constant decrease in abundance of silt, and an increase in abundance of sand (e.g., up to the maximum of ~20.83% for medium sand in DD #1) [1].

A more detailed view of the grain size distribution of DD #1 for every sample height separated in clay, silt, and sand is shown in Fig. 2. While the general distribution of sand is comparable in both DDs, the detailed distribution of clay and silt varies [1].

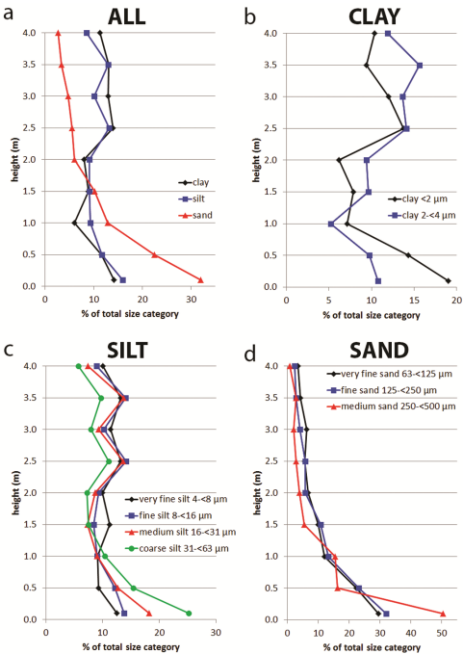

Figure 2: (a) Relative values of the total distribution of different particle sizes within DD #1. **(b-d)** Relative values of **(b)** clay, **(c)** silt, and **(d)** sand. From [1].

4. Discussion

The method used to sample active dust devils turned out to be very effective. With this method, even the smallest entrained particles (clay) of the dust devil will be preserved and are clearly visible on the non-textured bright adhesive tape under the microscope. Furthermore, the method allows a quick installation on-site and is transportable, which is important due to the fact that DDs can appear suddenly (giving a short reaction time for the sampler) and can move quickly over the surface.

Our measurements show that both DDs are comparable in their grain size distributions and their trends of mean values and medians. This is probably caused due to the same soil grain size distribution from which both DDs eroded material but also interesting in that both DDs had different sizes and intensities [1]. This is an indirect confirmation of simulations of [16-18] which showed that the dust flux of DDs are linked to their strength of pressure drops in their core, and not to their sizes.

Our measurements confirm observations from [19], that the majority (~65-80%) of lifted particles within a DD were smaller than 63 µm, and that only 1% of grains were relatively large (200-600 µm). In our experiments only ~1.8% for DD #1 and ~0.6% for DD #2 have sizes of 250 to <500 µm [1].

In contrast to [20], who presented a composition of a DD with ~42% fine sand and ~58% silt and clay, our measurements show a general smaller amount of lifted sand. Furthermore, our results show that between ~77 and ~89 wt% of the total particle load were lifted only within the first meter of the DDs, which is in good agreement with [21], and a direct evidence for the existence of a sand skirt. [21] concluded that ~10 wt% of the total lifted material contains grains between 0.1 and 10 µm, which will go into suspension. If we assume, that grains with a diameter <31 µm could go into suspension [1,3,7], our results show that only less than ~0.05-0.15 wt% can be entrained into the atmosphere [1], which is substantial less than proposed by [21]. However, these values represent between ~58.5% and ~73.5% of all lifted particles [1], because of the huge amount of entrained small particles. On Mars, the amount of lifted particles will be general higher as the surficial dust coverage is larger [22,23], although the atmosphere can only suspend smaller grain sizes (~<20 µm) [5] compared to Earth.

5. Conclusions

(I) Our measurements of DDs imply a similar or comparable internal structure, despite their different strengths and dimensions. **(II)** The vertical trend of decreasing particle size with height within DDs is confirmed and shows a nearly exponential decrease with height. **(III)** The existence of sand skirts in both DDs was directly verified. **(IV)** Our measurements show that only a small amount of the particle load can go into suspension, but these values represent between ~60% and ~70% of all lifted particles. We observed numerous larger dust devils each day (several hundred meters tall), which implies a much higher input of material into the atmosphere. **(V)** The size distribution within DDs probably represents the surficial grain size distribution they move over.

Acknowledgements

Both fieldworks were funded by Europlanet (TNA039 and 15-EPN-046), JR is funded by a Horizon 2020 Marie Skłodowska-Curie Individual Fellowship (H2020-MSCA-IF-2014-657452).

References

[1] Raack J. et al. (2017) *Astrobiology 17*, doi:10.1089/ast.2016.1544. [2] Thomas P.C. and Gierasch P.J. (1985) *Science 230*, 175-177. [3] Balme M. and Greeley R. (2006) *Rev. Geophys. 44*, RG3003. [4] Sinclair P.C. (1973) *J. Atmos. Sci. 30*, 1599-1619. [5] Newman C.E. et al. (2002) *JGR 107*, 5123. [6] Sinclair P.C. (1969) *J. Appl. Meteorol. 8*, 32-45. [7] Gillette D.A. and Sinclair P.C. (1990) *Atmos. Environ. 24A*, 1135-1142. [8] Mahowald N. et al. (2014) *Aeolian Res. 15*, 53-71. [9] Whelley P.L. and Greeley R. (2008) *JGR 113*, E07002. [10] Rossi A.P. and Marinangeli L. (2004) *GRL 31*, L06702. [11] Reiss D. et al. (2010) *GRL 37*, L14203. [12] Reiss D. et al. (2011) *Icarus 211*, 917-920. [13] Veverka J. (1976) *Icarus 27*, 495-502. [14] Malin M.C. and Edgett K.S. (2001) *JGR 106*, 23,429-23,570. [15] Udden J.A. (1914) *Bull. Geol. Soc. Amer. 25*, 655-744. [16] Neakrase L.D.V. et al. (2006) *GRL 33*, L19S09. [17] Neakrase L.D.V. and Greeley R. (2010) *Icarus 206*, 306-318. [18] Balme, M. and Hagermann, A. (2006) *GRL 33*, L19S01.[19] Oke A.M.C. et al. (2007) *J. Arid. Environ. 71*, 216-228. [20] Mattsson J.O. et al. (1993) *Weather 48*, 359-363. [21] Metzger S.M. et al. (2011) *Icarus 214*, 766-772. [22] Christensen, P.R. (1986) *JGR 91*, 3533-3545. [23] Ruff, S.W. and Christensen, P.R. (2002) *JGR 107*, 5127.

EPSC Abstracts
Vol. 11, EPSC2017-183, 2017
European Planetary Science Congress 2017

Integrated Scanning Electron Microscopy-Micro Raman spectrometer (SEM-Raman): future tool for planetary exploration

A. D. Shukla and D. Ray
Physical Research Laboratory (PRL), Ahmedabad 380009, India (anilds@prl.res.in)

Abstract

We identify and characterize the rock forming mineral using a newly installed, state of the art Scanning Electron Microscope integrated with Micro-Raman Spectrometer (SEM-Raman) at Physical Research Laboratory, Ahmedabad, India. The characteristic raman shifts (wave numbers) enable us acquiring the structural information and chemical fingerprint for any rock forming mineral. Due to capability of micron size sample analytical area, the unique SEM-Raman is also likely very useful for future planetary exploration for capable of analyzing the planetary materials (minerals, soils, etc) to understand the degree of crystallinity, unit cell information and also efficient in capable of scan the structural and compositional variants, e.g. the presence of different cations in different sites including the coordination configuration.

1. Introduction

Micro Raman spectroscopy is one of the powerful techniques for characterisation of Earth and planetary materials. Until now, Raman spectrometer has never been flown for planetary exploration except for NASA led Mars 2020 rover, which has planned to fly the UV Raman spectrometer to explore the martian surface with the aim for fine scale detection of minerals, organic molecules and potential biosignatures.

The motivation of studying the chromite include chromite is generally common in mantle derived ultramafic rocks also remotely detected in Moon and Martian surface or even in the meteorites. Based on possible target of planetary analogy, we have collected chromites from the ultramafic rocks from Nidar ophiolite complex exposed along the Indus Suture Zone of higher Himalaya [1]. This place is ideal for comparative planetology as the entire mantle sequence has been well exposed with variegated lower crustal and mantle units. In this short communication, we examine chromite mineral under Raman spectrometer as a utility tool to acquire the mineralogical and structural information.

2. Micro Raman Spectroscopy

The chromite sample was prepared using epoxy mound on a borosilicate glass slide which was earlier used for petrographic study. A few homogenous, smooth and clean areas are selected under Scanning Electron Microscope (SEM) (model JEOL IT300). The SEM is integrated with HybriScan Molecular Microscope (HSCMM_21) from HybriScan Technologies B.V. The Raman spectral signals are collected within the range 280 cm^{-1} to 2400 cm^{-1} with a spectral resolution better than 5 cm^{-1} Raman shift. The HSCMM_21 is a dispersive Raman micro spectrometer based on a 785 nm diode laser and back-thinned CCD detector. A scan stage with a fast 25 nm step resolution enables Raman imaging of user-defined areas. The optical microscope objective in the HSCMM_21 is designed for a vacuum environment and optimized for Raman light scattering. The light collection strength or numerical aperture is 0.65 and the spatial resolution of the confocal Raman micro-spectrometer is 1 µm in the lateral direction and 6 µm in the axial direction (for transparent materials). The Raman hyperspectral images are generated with 30 mW, 785 nm excitation, 1s exposure time. Measurements were taken on a 1 µm grid. A total number of 5508 spectra were acquired for raman analyses and finally yield the single average spectra (Fig.1).

3. Results & Discussion

There are five Raman-active vibrational modes in spinel $A_{1g}+E_g+3F_{2g}$ [2]. The three F_{2g} are often assigned as $F_{2g}(1)$, $F_{2g}(2)$ and $F_{2g}(3)$ whereas $F_{2g}(1)$ and $F_{2g}(3)$ correspond to the lowest and the highest Raman wave numbers respectively (Fig.2). The most strong band observations are common in the regions between 400-500 and 700-800 cm^{-1}. These two modes are assigned to E_g and A_{1g} modes, respectively. The bands around 200-300 cm^{-1}, 480-520 cm^{-1} and

600 cm^{-1} are diagnostic for first, second and third F_{2g} symmetry species.

In this study, the A_{1g} mode at ~685 cm^{-1} appears the strongest and well-defined mode with a shoulder near 650 cm^{-1} correspond to F_{2g} symmetry, followed by $F_{2g}(2)$ ~520 cm^{-1}(Fig. 2). The other peaks e.g. 446 and 610 $cm^{-1}$are rather weak, poorly defined and belong to E_g and F_{2g} respectively. We could observe that the most prominent the 685cm^{-1} which [1] is produced by the bonds of (Cr^{3+}, Fe^{3+}, Al^{3+})O_6 octahedra is present sample (Fig.3). The correlation between A_{1g} and chromite chemical composition can be expressed as polynomial function [3]. Using this correlation, our chromite data find a very good match with the EPMA data [4].

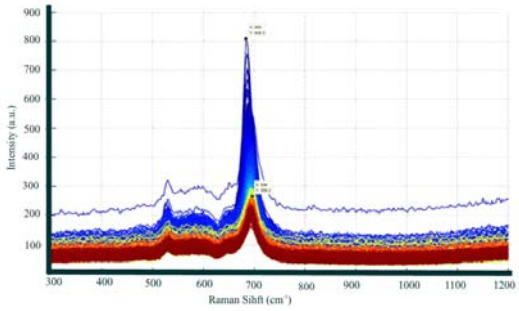

Figure 1: Spectra generated from a Raman spectral image. 1s per spectrum, 30 mW @785 nm excitation. The shift in the band around 685 cm^{-1} is obvious.

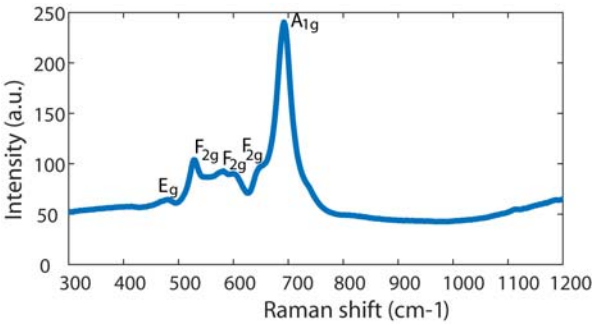

Figure 2: Identification of Raman bands with proper band assignment.

4. Summary and Conclusions

In summary, we find that the integrated SEM-Raman system is very useful for identification and characterisation of chromite. Further our results are consistent with the observed chemical composition and the vibration mode of $A^{3+}O_6$ (A=Al^{3+}, Cr^{3+}, Fe^{3+}),

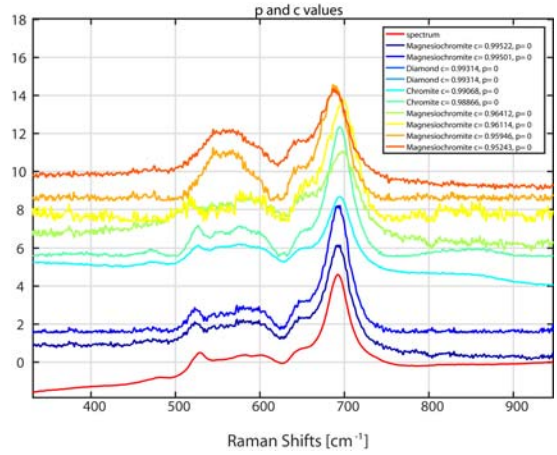

Fig. 3 Magnesiochromite as most likely or chromite after cluster average analysis and comparison with mineral database. The identification as diamond should be ignored as it is based on overlapping spectral regions without any features.

is likely the major contributor to the Raman peak of chromite. Thus, the raman peak also could be a useful guide to infer the chemical composition. Using micro Raman one can detect microbial extinct or extant life beyond the Earth vis-a-vis the planetary habitability.

Acknowledgements

We acknowledge Mr. Rolf Wolthuis, Hybriscan Technologies, BV, Arnhem, Netherlands for his generous help and support, in designing and performing the Raman analysis.

References

[1] Guillot, S., G. Garzanti, D. Baratoux, D. Marquer,G. Mahe´o, and J. de Sigoyer, Reconstructing the total shortening history of the NW Himalaya,Geochem. Geophys. Geosyst., 4(7), 1064, doi:10.1029/2002GC000484.2003

[2] Chopelas, A. and Hofmeister, A.M., Vibrational spectroscopy of alunite spinels at 1 atm and $MgAl_2O_4$ to over 200 kbar. Physics and Chemistry of Minerals, Vol. 18, pp. 279-293, 1991.

[3] Malézieux, J.M. and Piriou, B., Relation entre la composition chemique et le comportement vibrationel de spineless de synthese et de chromites naturalles en microscpectometrie Raman, Bulletin Mineralogue, Vol. 111, pp. 649-669, 1988.

[4] Wang, A., Kuebler, K.E., Jolliff, B.L. and Haskin, L.A. Raman Spectroscopy of Fe-Ti-Cr-oxides, case study: Martian meteorite EETA79001, American Mineralogist, Vol. 89, pp. 665-682, 2004.

EPSC Abstracts
Vol. 11, EPSC2017-451-3, 2017
European Planetary Science Congress 2017

In situ measurements of dust devil pressure drop magnitudes and vertical wind speeds

D. Reiss (1) and J. Raack (2)
(1) Institut für Planetologie, Westfälische Wilhelms-Universität, Münster, Germany, (2) School of Physical Science, STEM, The Open University, Milton Keynes, UK

1. Introduction

Dust devils are common on Earth and Mars. On Mars they significantly contribute to dust entrainment in the atmosphere. Meteorological signatures of vertical convective vortices (dust devils and dustless vortices) on the martian surface were detected with meteorological instruments on landers and rovers. The most prominent temporal signature of passing convective vortices is the reduced atmospheric surface pressure within the vortex. Such pressure drops were measured and analyzed at the Viking 2 [1], Pathfinder [2], Phoenix [3], and MSL [4, 5] landing sites. Recently, large datasets were obtained on Earth [e.g. 6, 7]. Pressure drop magnitudes are direct indicators for the intensity of dust devils and are directly related to the dust devil tangential speeds to a first approximation [e.g. 8]:

$V \approx \sqrt{\frac{RT_s\Delta p}{p_s}}$, where R is the atmospheric specific gas constant, T_s the ambient surface air temperature, Δp the pressure drop magnitude, and p_s the ambient pressure. Another important parameter is the vertical speed within dust devils, which is needed to calculate dust devil sediment fluxes on Earth and Mars [e.g. 9 – 11]. Vertical speeds within dust devils on Earth have been measured to be in the range of 0.1 – 10 ms^{-1} [e.g. 9, 12]. On Mars, vertical speeds were so far only estimated at the MER-A (Spirit) landing site tracking dust clods within individual dust devils from time-lapse imagery [10]. The estimated median vertical speeds are 1 ms^{-1} (season 2 and 3) and 1.6 ms^{-1} (season 1) [10]. However, no direct measurements of vertical speeds within dust devils on Mars are available to date. Based on terrestrial measurements of vertical and tangential speeds in dust devils by [12], [13] proposed that the vertical speed is about a quarter of the value of the maximum tangential speed. Establishing correlations between pressure drop magnitudes and vertical speeds in dust devils can help to improve dust devil sediment flux calculations on Earth and Mars where often only limited parameters can be measured (e.g., atmospheric pressure). For example, such relationships in combination with estimated or measured dust loads would enable the use of numerous pressure drop magnitude measurements for the calculation of dust devil sediment flux estimates at several landing sites on Mars.

2. Field site and Instrumentation

In 2016, we performed in situ dust devil measurements near Merzouga in southern Morocco. Amongst other parameters, we measured atmospheric pressure and vertical wind speed at heights of 0.15 m above the surface. We used 5 fixed meteorological stations spaced by 5 m and logging at a sampling rate of 20Hz. Figure 1 shows an example of a dust devil directly crossing one station as well as an example of measured atmospheric pressure and vertical wind speed during a passage of a dust devil. The high time sampling resolution at 20 Hz enables us to detect even small (~1m in diameter) and fast moving dust devils. Atmospheric pressure was measured with a Bosch BMP280 digital pressure sensor set to ultra-high resolution mode (pressure oversampling = 16, temperature oversampling = 2, $t_{standby}$ = 0.5 ms, IRR filter = off) which results in a pressure resolution of 0.16 Pa, a relative accuracy of 12 Pa, and a measurement time of 40 ± ~3ms. The vertical wind speed was measured with low-cost Modern Device Rev. P hot-wire anemometers with a accuracy of ±0.5 ms^{-1} [14]. We also tested the hot-wire anemometers against an industrial cup anemometer at different sampling frequencies (1, 10, and 20 Hz) showing accurate measurements within the accuracy of ±0.5 ms^{-1}. Each anemometer was mounted within a pipe (5 × 10 cm in dimensions) to minimize noise from horizontal winds. All data were directly logged onto a SD-card using an Arduino Leonardo microprocessor with a data logger shield. In addition, the meteorological stations were monitored with a GoPro3 at a sampling rate of 1 Hz to document and constrain the path of dust devils in relation to the fixed stations.

3. Results

Figure 2A shows our measured peak pressure drop magnitudes versus peak vertical speeds of 13 dust devils which directly crossed one of the meteorological stations. Our study indicates that the vertical speed is about 0.06×ΔP. For comparison with other studies we calculated the peak tangential speeds from our peak pressure drop magnitudes (see equation above). Figure 2B shows the tangential speeds versus vertical speeds of our study in 2016 in comparison with other studies. Our study indicates that the vertical speed is about half the tangential speed and in good

agreement with studies by [15], [16], and [17]. The reason for the discrepancy of our study with early studies by [12] and [18] indicates that the vertical speed is about one fifth of the tangential speed is unclear but might be, for example, due to differences in instrumentations or sampling rates. We are currently planning another field campaign using fixed as well as mobile stations to measure pressure drop magnitudes and vertical speeds at different heights to obtain a statistically more robust dataset.

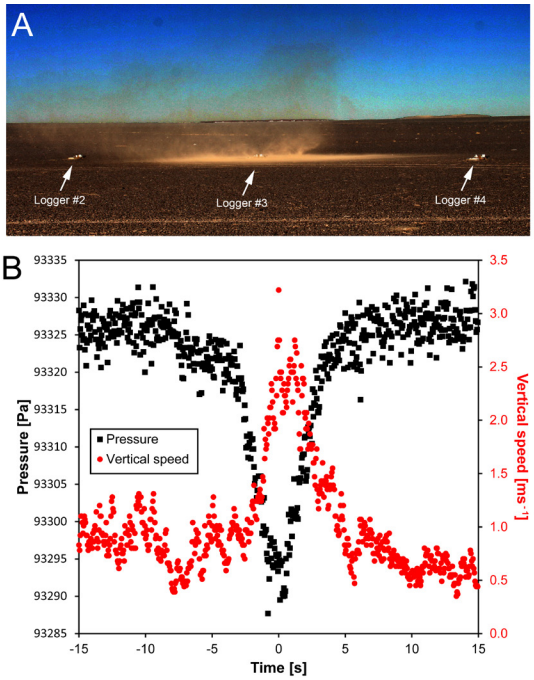

Figure 1: (A) Example of a dust devil directly passing over one of the fixed meteorological station. (B) Example of measured atmospheric pressure and vertical speed during a passage of a dust devil directly crossing one of the fixed meteorological station.

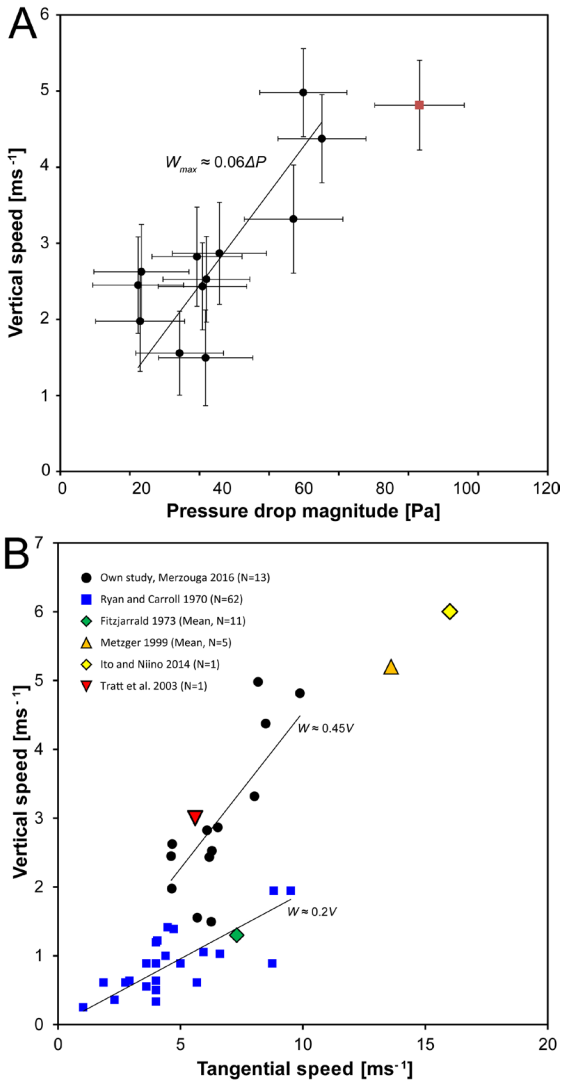

Figure 2: Relationships between dust devil vertical speeds to pressure drop magnitudes and tangential speeds. (A) Pressure drop magnitudes versus peak vertical speeds derived from dust devil cores passing directly over the sensors of fixed meteorological stations in 2016 near Merzouga (Morocco). The red square data point indicates recalculated pressure drop magnitude because the pressure sensor malfunctioned during the passage of the dust devil before the minimum pressure was reached. Indicated errors are combined instrument accuracy and peak value fitting uncertainties. (B) Comparison of our dust devil calculated peak tangential speeds versus measured peak vertical speeds with other studies.

References

[1] Ringrose, T.J. et al. (2003) Icarus 163, 78–87. [2] Murphy, J.R. and Nelli, S. (2002) Geophys. Res. Lett. 29, 2103. [3] Ellehoj, M.D. et al. (2010) J. Geophys. Res. 115, E00E16. [4] Kahanpää, H. et al. (2016) J. Geophys. Res. 121, 1514–1549. [5] Steakley, K. and Murphy, J. (2016) Icarus 278, 180–193. [6] Lorenz, R.D. and Lanagan, P.D. (2014). Boundary-Layer Meteorol. 153, 555-568. [7] Lorenz, R.D et al. (2015) Aeolian Res. 19, 183–194. [8] Rennó, N. O. et al. (2000) J. Geophys. Res. 105, 1859–1865. [9] Metzger, S.M. et al. (2011) Icarus 214, 766–772. [10] Greeley, R. et al. (2010) J. Geophys. Res. 115, E00F02. [11] Reiss, D. et al. (2014) Planet. Space Sci. 93–94, 54–64. [12] Ryan, J.A. and Carroll, J.J. (1970) J. Geophys. Res. 75, 531–541. [13] Balme, M. and Greeley, R. (2006) Rev. Geophys. 44, RG3003. [14] Prohasky, D. and Watkins, S. (2014) Australasian Fluid Mechanics Conference, Melbourne, Australia. [15] Metzger, S.M. (1999) PhD-Thesis, Univ. of Nev., Reno, 208 p. [16] Tratt, D.M. et al. (2003) J. Geophys. Res. 108, 5116. [17] Ito, J. and Niino, H. (2014) Sola 10, 108–111. [18] Fitzjarrald, D.E. (1973) J. Appl. Meteorol. 12, 808–813.

Acknowledgements

This study was supported by Europlanet grant E15-EPN-046 – Europlanet 2020 RI TA (2016). Europlanet 2020 RI has received funding from the European Union's Horizon 2020 research and innovation programme under grant agreement No 654208. We thank Gian G. Ori and Kamal Taj-Eddine from Ibn Battuta Centre (Marrakesh) for their great support of the field work.

EPSC Abstracts
Vol. 11, EPSC2017-785, 2017
European Planetary Science Congress 2017

Desert spring mounds: a potential analogue to Martian arid environments?

F. Franchi[1], S. Frisia[2]
1. Botswana International University of Science and Technology, Palapye, BOTSWANA (franchif@biust.ac.bw)
2. School of Environmental and Life Sciences, University of Newcastle, AUSTRALIA

Abstract

Spring carbonates have been often considered as putative analogues of Martian arid environments. On Earth these are believed to form by the interaction of highly saline water and microbial communities, which favor the formation of authigenic micrite. Here we present new data from spring mounds in the western Makgadikgadi Pan (Botswana) and the Great Artesian Basin (South Australia). In both areas, upwelling of ground water give rise to mounds and layered deposits which are close morphological analogues of landforms documented on Mars. The authigenic carbonates and evaporites associated with the spring mounds retain evidence of microbial microfabric founded elsewhere, pointing to the potential existence of similar microbial in the extreme Martian conditions.

1.Introduction

Earth geological record preserves fossil of living systems that show adaption of life to extreme and unique environments [2] such as desert spring mounds (Fig. 1 A, B). The study of these systems provides insight into the nature of rock/life interactions on Earth [1], and may give clues to life forms could have been preserved in the rock record of Mars [13]. Occurrences of alleged spring mounds have been recently reported for the equatorial region of Mars [4, 9, 11] (Fig. 1C). These landforms are commonly exposed within major craters filled by sedimentary units collectively referred to as Equatorial layered Deposits (ELDs). It has been hypothesized that ELDs have been deposited by cyclical groundwater upwelling [4].

Similarly to other continental microbially induced, carbonates, desert spring mounds exhibit micrite and microsparite layers suitable for petrographic and geochemical investigation at micro- to nano-metre scale [5]. Critically, crystallization pathways in the presence of microbes, seem to occur via non-classical nucleation and growth through mechanism common both to inorganic and bio-mediated processes. However, purely inorganic carbonates, where organic compounds are absent, seem to be characterized by diagenetic ripening [5]. This implies that the characterization of the spring mound carbonates potentially provide insight on their formation.

2.Study area

Spring sediments in arid regions of Botswana and South Australia (Fig. 1A, B) occur along the western margin of the Makgadikgadi Pan (MKP) [8] and along the western margin of the Great Artesian Basin (GAB) [3, 6, 7], respectively. There, the groundwater flux reaches the surface favoring deposition of carbonates and evaporites organized in mounds characterized by tufa (Fig. 1B) and travertines [3, 6].

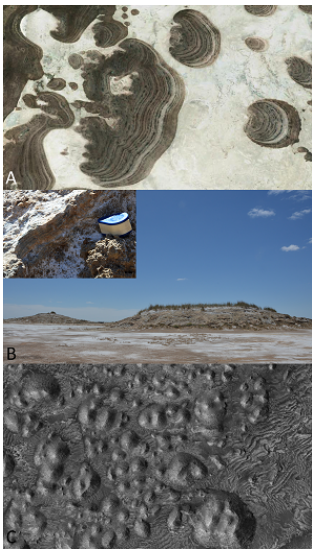

Figure 1: A) MKP mounds (Google Earth). B) GAB mounds characterized by tufa (inset). C) Firsoff crater mounds (ESP_020679_1820).

3.Methods

The present research has commenced by scrutinizing the outer morphologies of the mounds. Satellite imagines (Google Earth) of terrestrial landforms were compared with remote sensing data. The NASA Context Camera (CTX) images were combined with high-resolution HiRISE (High Resolution Imaging Science Experiment on Mars Reconnaissance Orbiter) and High Resolution Stereo Camera (HRSC) data.

Preliminary field work was carried by FF in October 2016. Samples of sediments and rocks have been collected and preliminary investigated by X-ray diffraction (XRD), standard optical microscopy and Scanning Electron Microscopy (SEM-EDS). This is the basis for the next step, which will include High Resolution Transmission Electron Microscopy and elemental mapping.

4.Results and Discussion

Along the western margin of the GAB, where groundwater reaches the surface microbialite (Fig. 1B), travertines and phytoherm framestone tufa occur. Mounds consist of aeolian dust cemented by variable amounts of calcite and dolomite. The evaporation rates in the area average 2.5 m/yr with a volume of water loss through evapotraspiration ranging between 6% and 33% [6]. GAB spring water is highly alkaline (high Na^+ and Cl^- and low HCO_3^- contents), although strongly acidic spring water ($pH<2.5$) have been also described [7]. In analogy to Triassic and present evaporative and alkaline environments, nucleation and growth of micrite, and specifically dolomicrite, is likely to be favored by organic compounds [10]. The poorly known MKP mounds from Central Botswana (Fig. 1A), which were thought to be wind dunes, bear evidence of cyclic groundwater upwelling [8] potentially conducive to microbial bio-mediated precipitation of salts.

Whilst the terrestrial springs mounds under investigation mostly consist of wind dust, carbonates and evaporite minerals, Mars spring deposits are dominated by sulphates and minor amount of carbonates [12] precipitated by cyclical upwelling of saline groundwater [4]. Outcrop-scale investigation of Martian sedimentary rocks [12] revealed that aeolian sediments are cemented by evaporite mineral deposited in a playa-lake setting. Therefore, if we seek an understanding of life on Mars, it becomes crucial to unravel processes that shape spring deposits on GAB and MKP.

5.Conclusions

Spring sediments deposited in terrestrial arid environments of MKP and GAB are morphological analogues of landforms which are believed to be formed in playa-like environments on Mars. GAB spring carbonates preserve micromorphologies and mineral associations which is typical of those of arid environments of Pangaea “microbialites”.Preliminary data reveal that layering of carbonates may reflect a change in the mineralization, and, likely, changes in the influence of microbial activity. Detailed micro and nanostructural study of these carbonates will shed light onto both bio-mediated and inorganic processes conducive to the formation of Martian-like mounds.

Acknowledgements

Field work has been supported by the Explorer Club Exploration Found Grant (Mamont Scholars).

References

[1] Brocks, J.J., et al., 1999. Science 285 (5430), 1033-1036.

[2] Burns, B.P., et al., 2009b. Precamb. Res. 173, 10-18

[3] Clarke, J.D.A., Bourke, M.C., 2011. Analogs for Planetary Exploration. Geol. S. Am. S. 483, pp. 231-247.

[4] Franchi, F., et al., 2014. Planet. Space Sci., 92, 34-48.

[5] Frisia et al., EGU 23-28 April 2017, Vienna, Austria, 2017.

[6] Keppel, M.N., et al., 2012. Chem. Geol. 296-297, 50-65.

[7] Love, A.J., et al. 2013. Proc. Earth Planet. Sci. 7, 521-524.

[8] McFarlane, M.J., Long, C.W., 2015. Quatern. Int. 372, 108-119.

[9] Pondrelli, M., et al. Geol. Soc. Am. Bull., B31225.1, 2015.

[10] Preto et al., 2015 Sedimentology, 62, 697-716

[11] Rossi, A.P., et al. 2008. J. Geophys. Res. 113, E08016.

[12] Squyres, S.W., Knoll, A.H., 2005. Earth Planet. Sci. Lett. 240, 1-10.

[13] Walter, M.R., Des Marais, D.J., 1993. Icarus 101,129-143.